Progress in Nuclear Lattice Effective Field Theory

Ulf-G. Meißner[0000−0003−1254−442X]
and
Fabian Hildenbrand[0000−0002−3763−3747]

Abstract In this chapter, we present recent progress in nuclear structure and reaction theory using the framework of Nuclear Lattice Effective Field Theory. Topics include the study of the radii of certain oxygen isotopes, the role of three-nucleon forces in neutron-alpha scattering, the study of multi-neutron correlations in light nuclei as well as the investigation of multi-strangeness matter as seen in hypernuclei and neutron stars. Finally, we discuss some novel results on the fine-tunings of fundamental parameters in radiative α-particle capture on ^{12}C at astrophysical energies.

Keywords Nuclear theory · Lattice simulations · Chiral effective field theory

1 Short introduction to NLEFT

Abstract In this section, we give a very brief introduction into the framework of Nuclear Lattice Effective Field Theory (NLEFT). NLEFT is a powerful tool that allows to address problems in nuclear theory with high precision, some of them being unsolvable with conventional continuum approaches.

Understanding the formation of strongly interacting systems such as atomic nuclei from first principles calculations is still one of the biggest challenges within contemporary theoretical physics. While the theory of the strong interactions, Quantum Chromodynamics (QCD), is well tested in many processes, the matter that leads to life in our Universe is based on nuclei, which are self-bound systems of nucleons (protons and

Ulf-G. Meißner
Helmholtz-Institut für Strahlen- und Kernphysik and Bethe Center for Theoretical Physics, Universität Bonn, D-53115 Bonn, Germany and Institute for Advanced Simulation (IAS-4), Forschungszentrum Jülich, D-52425 Jülich, Germany e-mail: meissner@hiskp.uni-bonn.de

Fabian Hildenbrand
Institute for Advanced Simulation (IAS-4), Forschungszentrum Jülich, D-52425 Jülich, Germany e-mail: f.hildenbrand@fz-juelich.de

neutrons). As the nucleons themselves consist of quarks and gluons, and hence are not fundamental degrees of freedom, the forces between nucleons are not completely given in terms of two-body interactions, but include three-body and higher order interaction terms. Much progress in the understanding of the structure and dynamics of nuclei has been made in the context of Nuclear Lattice Effective Field Theory (NLEFT) [1], which combines the so successful low-energy chiral effective field theory of QCD with stochastic methods (Monte Carlo simulations). While direct calculations of nuclei based on quarks and gluons in the framework of lattice QCD are essentially impossible due to the severe sign problem, formulating the nuclear forces in terms of protons, neutrons and pions is not only more appropriate, but also comes with the added value of the approximate Wigner SU(4) spin-isospin symmetry of the underlying nuclear interactions. This symmetry in fact suppresses the sign oscillations strongly, and in the limit of an exact Wigner SU(4) symmetry, spin-isospin saturated nuclei like e.g. ^{4}He are free of any sign oscillation [2]. In NLEFT simulations, Euclidean space-time is discretized on a torus of volume $L^3 \times L_t$, where L is the side length of the spatial dimensions, and L_t denotes the extent of the Euclidean time dimension. The lattice spacing in the spatial (temporal) dimensions is a (a_t). The maximal momentum on the lattice is $p_{\max} \equiv \pi/a$, which serves as the UV regulator of the theory. Nucleons are point-like particles on the lattice sites, and the interactions between nucleons (pion exchanges and contact terms) are treated as insertions on the nucleon world lines via auxiliary-field representations. For a schmematic representation, see Fig. 1. Properties of multi-nucleon systems are

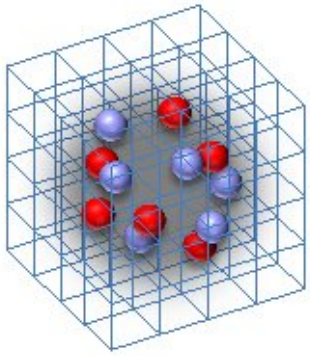

Fig. 1 Schematic representation of a nucleus on the lattice, here ^{12}C consisting of six protons and six neutrons. Protons and neutrons are depicted by red and blue spheres, respectively. The lattice spacing a is the distance between two adjacent lines and the total volume for this case is $V = (4a)^3$.

computed by means of the projection Monte Carlo (MC) method. Each nucleon is treated as a single particle propagating in a fluctuating background of pion and auxiliary fields. Both local and non-local smearings are applied to the nucleon creation and annihilation operators. Euclidean time projection is started from some initial wave function Ψ_A for Z protons and N neutrons (with $A = Z + N$ the atomic number). One calculates the ground state energy and other properties from the correlation function $Z(t) \equiv \langle \Psi_A | \exp(-\tau H) | \Psi_A \rangle = \mathrm{Tr}\{M^{L_t}\}$, in the limit of large Euclidean projection time τ, with M the normal-ordered transfer-matrix operator and L_t the number of Euclidean time steps. Higher-order contributions are computed as perturbative corrections to the LO results. A much more detailed description is given in the monograph [1].

2 Ab initio study of the radii of oxygen isotopes

Abstract Understanding the nuclear charge radii from *ab initio* nuclear theory remains a formidable challenge. Continuum approaches face the so-called radius problem, namely a systematic underprediction of the charge radii, seen e.g. in the chains of oxygen and calcium isotopes. Here, we show how this is overcome in NLEFT.

Accurate *ab initio* predictions of nuclear charge and matter radii remain a long-standing challenge in nuclear theory, owing to strong many-body correlations and severe Monte Carlo sign problems, see e.g. Refs. [3, 4, 5]. In our earlier work, we had already shown that within NLEFT using the wave-function matching apporach [6], this problem is overcome, but the accuracy of some predictions for the charge radii needed improvement due to the sign problem induced by the pinhole algorithm. The latter is the tool to fix the center-of-mass on the lattice and thus allows to calculate the charge distributions and the pertinent moments, like the radii. For details, see Refs. [7, 6]. In Ref. [8], we have addressed this challenge for the oxygen isotopic chain by performing first-principles calculations of the charge and matter radii of $^{16\text{–}20}$O within NLEFT using high-fidelity chiral interactions at next-to-next-to-next-to-leading order (N^{3}LO). To overcome the prohibitive sign oscillations encountered in conventional radius calculations, we introduce the *partial pinhole algorithm*, which systematically reduces the rank of the many-body density operator and enables stable simulations at significantly larger imaginary times. By combining the partial pinhole algorithm with the wave-function matching method, we achieve a substantial reduction of statistical uncertainties and are able to resolve subtle isotopic trends in nuclear radii. Our results accurately reproduce the experimentally observed charge radii of ^{16}O, ^{17}O, and ^{18}O, including the pronounced increase from ^{17}O to ^{18}O that has remained elusive in other *ab initio* approaches, see Fig. 2. Furthermore, we provide a first-principles prediction for the

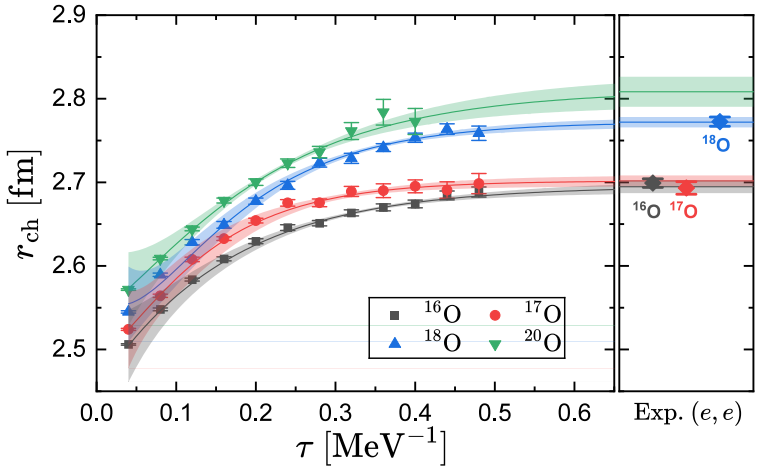

Fig. 2 Results for the charge radii for the oxygen isotope chain compared to experiment. For more details, see also Ref. [8].

charge radius of the neutron-rich isotope ^{20}O, $r_{\rm ch}(^{20}{\rm O}) = 2.810(32)$ fm. The calculated matter radii show excellent agreement with values extracted from low-energy electron and proton scattering, while revealing significant discrepancies with those inferred from interaction cross sections, thereby highlighting model-dependent ambiguities in experimental extractions. This work was published in *Physical Review Letters* [8].

3 Ab initio lattice study of neutron-alpha scattering with chiral forces at N^{3}LO

Abstract In this section, we scrutinize the three-nucleon forces underlying the successful calculations of nuclear binding energies, radii and other observables, by considering neutron-alpha scattering. The occuring disprecancy in the spliiting of the two P-waves shows that further refinements of these forces are required.

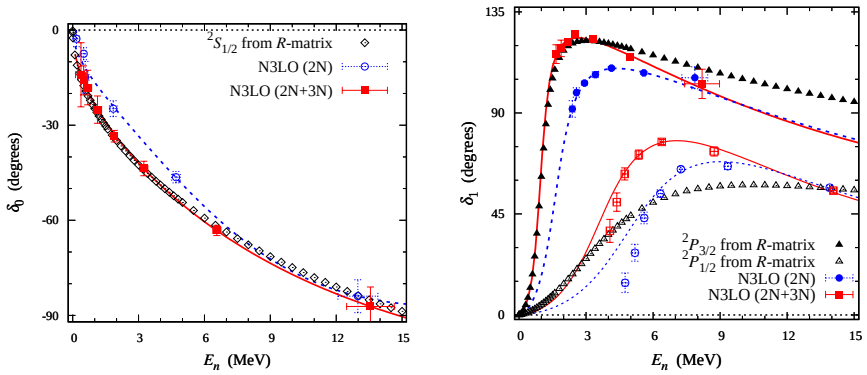

Fig. 3 Neutron-alpha phase shifts at N^{3}LO as functions of the neutron laboratory energy E_n. **Left:** $^2S_{1/2}$. **Right:** $^2P_{3/2}$ and $^2P_{1/2}$. Symbols with error bars are lattice results, blue circles denote the N^{3}LO (2N only) results, and red squares denote N^{3}LO (2N+3N) results. Solid red curves are effective range expansion (ERE) fits to the full N^{3}LO (2N+3N) lattice data, and dashed blue curves are ERE fits to the the N^{3}LO (2N sole) lattice points. Black symbols denote empirical R-matrix phase shifts [12] (diamonds for $^2S_{1/2}$ and filled and open triangles for $^2P_{3/2}$ and $^2P_{1/2}$).

It is well established that neutron-alpha (n-α) scattering is a fine probe of three-nucleon forces that play such an important role in precision calculations of atomic nuclei, see e.g. Ref. [9]. The first *ab initio* lattice calculation of n-α scattering employing NLEFT with chiral interactions up to next-to-next-to-next-to-leading order (N^{3}LO) was presented in Ref. [10]. By utilizing the high-fidelity chiral Hamiltonian developed in our previous work, we computed scattering phase shifts in the S- and P-wave channels via the Lüscher finite-volume method [11]. Our findings show excellent agreement with empirical R-matrix analyses in the $^2S_{1/2}$ and $^2P_{3/2}$ channels, while highlighting persistent discrepancies in the $^2P_{1/2}$ channel at neutron energies above $E_n \simeq 5\,$MeV, see also Fig. 3. We systematically investigate these discrepancies using a simplified

neutron-alpha model, confirming that the issue is not due to methodological limitations of the Lüscher approach. Furthermore, we revisit and refine our three-nucleon force (3NF) parameterization procedure by explicitly incorporating neutron-alpha scattering data, underscoring the stability of nuclear binding-energy predictions and identifying areas for further refinement of lattice three-nucleon forces. This comprehensive analysis provides significant benchmarks for state-of-the-art *ab initio* nuclear theories and advances our understanding of nucleon-nucleus scattering processes, particularly emphasizing the importance of accurately formulating three-nucleon forces in nuclear lattice calculations. This work has been published in *Journal of Physics G* [10].

4 Multi-neutron correlations in light nuclei via ab-initio lattice simulations

Abstract There is large experimental activity to search for a four-neutron bound state or resonance, the so-called tetraneutron. We propose a new method to deal with such multi-neutron configurations in light, neutron-rich nuclei. In particular, we show that four neutrons preferably appear in dineutron-dineutron configurations, which complicates the search for tetraneutons.

The quest to understand multi-neutron systems has a long history and recent experimental efforts aim to probe candidate four-neutron configurations in neutron-rich light nuclei such as ^{8}He and ^{7}H via quasi-free knockout reactions, see Ref. [13] for a review. However, the ground-state energies of the hydrogen isotopes ^{6}H and ^{7}H are not yet well constrained, with substantial discrepancies across experimental analyses and theoretical predictions. Using *ab initio* NLEFT with an ensemble of 282 chiral two- and three-nucleon forces, we perform an uncertainty-quantified analysis of the ground-state (g.s.) energies of ^{6}H and ^{7}H, finding $E_{\text{g.s.}} = -4.94 \pm 0.14$ MeV and -5.29 ± 0.16 MeV, respectively, see Fig. 4 (left panel). The marginal posteriors suggest single-neutron separation energy $S_n(^{7}\text{H}) = 0.35 \pm 0.32$ MeV, disfavoring sequential $^{6}\text{H} + n$ decay and pointing towards direct $t + 4n$ emission. Intrinsic densities indicate triton- and α-like clusters in ^{7}H and ^{8}He, respectively. By computing two-body and reduced four-body correlation functions, we find that the valence neutrons in the surface region of these systems form compact dineutrons that predominantly organize into symmetric dineutron-dineutron configurations, with only a small but non-negligible fraction assembling into more compact tetraneutron-like substructures, see Fig. 4 (right panel). In ^{7}H, these components account for roughly 95% and 5% of the sampled four-neutron configurations, respectively, and ^{8}He exhibits a similar hierarchy. For these configurations, we also extract the corresponding spatial and angular correlation patterns among the nucleons. These results provide nuclear-structure insights into the debate surrounding four-neutron clusters and complement ongoing experimental searches for tetraneutron signatures in light nuclei. The preprint is available at Ref. [14] and is submitted to *Physicsal Review Letters*.

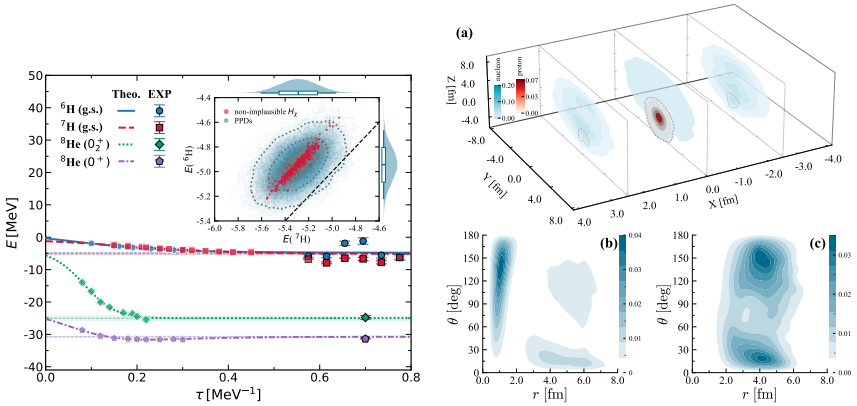

Fig. 4 Left: Calculated and experimental g.s. energies of ^{6,7}H, and the 0^+ and $0_2{}^+$ state energies of ^{8}He. Colored markers overlaid on the corresponding curves indicate the calculated energies versus Euclidean time τ, with statistical uncertainties. The curves represent the τ-extrapolation fits, and horizontal dashed lines denote the extrapolated $\tau \to \infty$ energies with their statistical uncertainties. Experimental data are shown as symbols labeled "EXP" in the legend. **Inset:** The red circles represent the g.s. energies of ^{6,7}H from non-implausible prior samples obtained via history matching, including uncertainties. Posterior samples are shown as pale blue points, with dashed lines indicating the 1σ and 2σ credible intervals. The dashed black line denotes the condition $E(^6\mathrm{H}) = E(^7\mathrm{H})$. Marginal distributions are shown along each axis, with medians indicated by ticks and thick and thin bars representing the 1σ and 2σ credible intervals, respectively. **Right:** (a) Intrinsic nucleon (blue) and proton (red) densities of the ^{7}H ground state, visualized as slices at $x = 0$ and $x = \pm 2.5$ fm. The red dashed line marks the maximal spatial extent of the identified triton cluster. (b) Two-neutron correlation density of all neutrons in the ^{7}H ground state, with r defined relative to the center-of-mass (c.m.) of the core. (c) Two-neutron correlation density of the four valence neutrons, with r defined with respect to the c.m. of the ^{7}H.

5 Multi-strangeness matter from ab initio calculations

Abstract In this section, we show that within the framework of NLEFT one can systematically describe the properties of hypernuclei and of neutron stars in the presence of hyperons, solving the so-called hyperon puzzle. To achieve the high densities as they appear in the interior of neutron stars, we construct a minimal nuclear interaction that also allows for the inclusion of Λ hyperons by an elegant formulation of the baryonic auxiliary fields.

Hypernuclei and hypernuclear matter bridge nuclear structure in the strangeness sector with the astrophysics of neutron stars, where hyperons are expected to appear at high densities and significantly influence key astrophysical observables. In Ref. [15], we have presented the first *ab initio* calculations that provide a unified description of both single- and double-Λ hypernuclei across the light to medium-mass range, the equation of state for β-stable hypernuclear matter, and the resulting neutron star properties. Despite the formidable complexity of quantum Monte Carlo (QMC) simulations involving multiple baryonic degrees of freedom, we achieve – by combining NLEFT with a newly developed auxiliary-field QMC algorithm – the first sign-problem-free *ab initio* QMC simulations of hypernuclear systems containing arbitrary numbers of neutrons, protons,

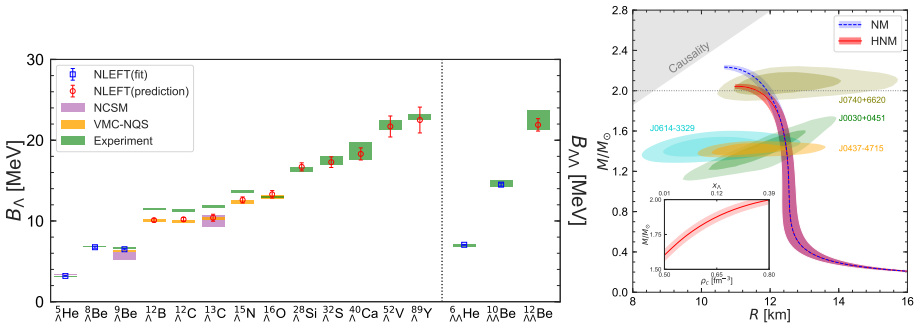

Fig. 5 Left: Single-Λ and double-Λ separation energies for hypernuclei. Hypernuclei used to fit the $NN\Lambda$ and $N\Lambda\Lambda$ forces are depicted by blue squares. Predictions are shown as red circles. Error bars represent the combined statistical and systematic uncertainties. NLEFT results are compared with experimental data from the Hypernuclear Database (green) [16], and with recent *ab initio* predictions from the variational Monte Carlo method based on neural network quantum states (VMC-NQS, orange) [17] and the no-core shell model (NCSM, purple) [18]. **Right:** Neutron star mass-radius relation. The gray horizontal dotted line marks $2M_\odot$. The inner and outer shaded contours indicate the mass-radius constraints from the NICER analysis. The inset shows the neutron star mass as a function of central density, together with the corresponding Λ-hyperon particle fractions.

and Λ hyperons. These simulations incorporate all relevant two- and three-body interactions, and all parameters of the interactions involving hyperons are determined from the binding energies of single- and double-Λ hypernuclei, see the left panel of Fig. 5. This work also eliminates reliance on the symmetry-energy approximation, commonly used to interpolate between symmetric nuclear matter and pure neutron matter. Our *ab initio* calculations reproduce hyperon separation energies, yield a maximum neutron star mass consistent with observations, predict tidal deformabilities compatible with gravitational-wave measurements, and provide a trace anomaly in agreement with Bayesian constraints, see Fig. 5 for the mass-radius relation in comparison to recent NICER measurements (right panel). Note further that hyperons appear at a density of about 0.5 fm^{-3} and have a large fraction inside the neutron star core (as shown in the inset in the right panel of Fig. 5). By seamlessly connecting the physics of finite hypernuclei and infinite hypernuclear matter within a single *ab initio* framework, this work establishes a direct microscopic link between hypernuclear structure, the composition of dense matter, and the astrophysical properties of neutron stars. The preprint of this work is available in Ref. [15] and currently under consideration in *Physical Review Letters*.

6 Fine-tunings in radiative α-particle capture on ^{12}C at astrophysical energies

Abstract Here, we investigate the sensitivity of the radiative α-particle capture on ^{12}C, which generates ^{16}O in stars, on the electromagnetic fine-structure constant. We find

that only very small variations are consistent with the data, which sets much stronger bounds on fine-tunings in nucleosynthesis than found earlier.

Fine-tunings appear in most fields of physics and often pave the way to new approaches to the pertinent problems, see e.g. Ref. [19]. In earlier work, we had systematically studied the dependence of element generation in the Big Bang and in hot, old stars, especially the location of the Hoyle state in carbon, that enables life on Earth as we know it, on the fundamental parameters of the Standard Model, such as the electromagnetic fine-structure constant or the light quark masses. With respect to variations of the electromagnetic fine-structure constant α, we found only broad limits of about 2% from primordial nucleosynthesis [20] and about 5% from the location of the Hoyle state in the spectrum of ^{12}C [21]. Differently from this, little is known about the fine-tunings in radiative alpha-particle capture on carbon, $^{12}\mathrm{C}(\alpha,\gamma)^{16}\mathrm{O}$, at astrophysical energies, the so-called holy grail of nuclear astrophysics. More precisely, the energy is set by the so-called Gamov energy, $E_G \simeq 0.3\,\mathrm{MeV}$, which is the energy that maximises the tunneling of a charged particle (here, the alpha particle) through the Coulomb barrier of the nucleus. Utilizing results from cluster effective field theory for this reaction [22], we find that the low-energy data of the astrophysical S-factor allow for only very small variations in the electromagnetic fine-structure constant α, namely $|\delta\alpha/\alpha| \leq 0.2\,‰$, in both the $E1$ and the $E2$ radiative capture, see Fig. 6. This work is available in [23] and is accepted for publication in *Communications in Theoretical Physics*.

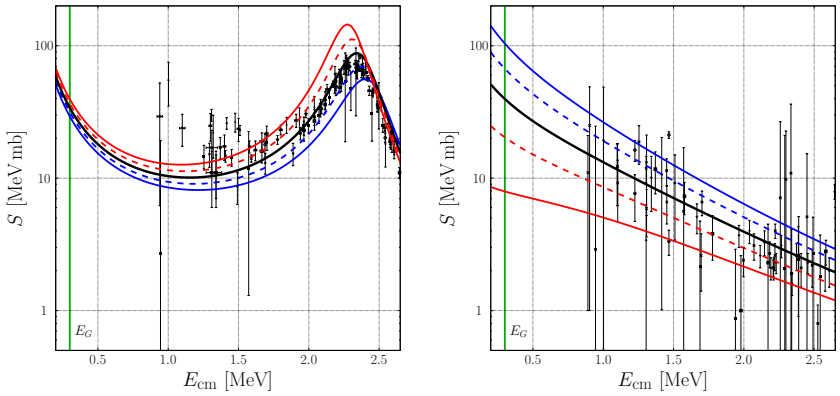

Fig. 6 Fine-structure constant variation of the astrophysical S-factor of the radiative capture reaction $^{12}\mathrm{C}(\alpha,\gamma)^{16}\mathrm{O}$. The result for the nominal value of α is displayed in black. The blue (dashed) curves correspond to $\delta = -0.0002(-0.0001)$; the red (dashed) curves to $\delta = 0.0002(0.0001)$. The position of the Gamow energy at $E_G \simeq 0.3\,\mathrm{MeV}$ is indicated by a vertical green line. **Left/right panel:** $E1/E2$ transition.

Acknowledgements We wish to thank all members of the NLEFT Collaboration for useful discussion that shaped the research presented in these chapters. This work is part of the EXOTIC grant and was supported in part by the European Research Council (ERC) under the European Union's Horizon 2020 research and innovation programme (grant agreement No. 101018170) and by the MKW

NRW under the funding code NW21-024-A The work of UGM was also supported by the CAS President's International Fellowship Initiative (PIFI) (Grant No. 2025PD0022). The authors gratefully acknowledge the computing time provided on the high-performance computer HoreKa by the National High-Performance Computing Center at KIT (NHR@KIT). This center is jointly supported by the Federal Ministry of Education and Research and the Ministry of Science, Research and the Arts of Baden-Württemberg, as part of the National High-Performance Computing (NHR) joint funding program (https://www.nhr-verein.de/en/our-partners). HoreKa is partly funded by the German Research Foundation (DFG). Further computational resources provided by the Gauss Centre for Supercomputing e.V. (www.gauss-centre.eu) for computing time on the GCS Supercomputer JUWELS at Jülich Supercomputing Centre (JSC) are also gratefully acknowledged.

Competing Interests The authors have no conflicts of interest to declare that are relevant to the content of any chapter.

Appendix A: Performance parameters and machine usage

For typical NLEFT calculations, the relevant performance parameter is generation and measurement of configurations (of nucleons and auxliary fields) per core per hour. Since a node on HOREKA has 76 cores, we present here result in node hours. We show the results for a typical project as presented in Chapter 2. The calculations in the other projects scale in a similar fashion.

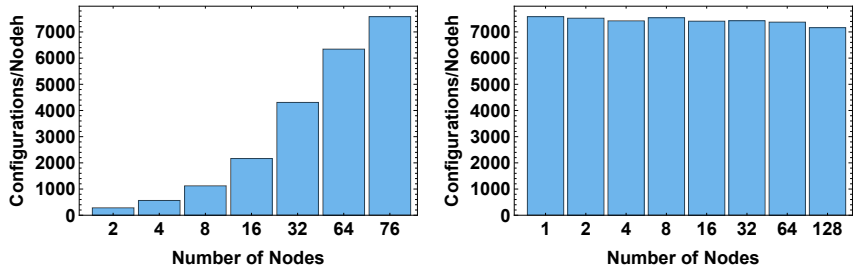

Fig. 7 Perfomance parameters for a calculation of ^{16}O at $L_t = 100$ at $L = 10$ in lattice units. **Left panel:** Performance for one node, increasing from the minimal possible node occupation (2 cores) to full usage (76 cores). **Right panel:** Weak scaling utilizing 76 cores per node (optimal value) starting from one node to 128 nodes.

On the left side of Fig. 7, we show the scaling using only one node of HOREKA (2x Intel Xeon Platinum 8368) utilizing up to 76 CPU cores. Clearly using all available cores provides the best performance. The performance gain, however, slows down for more than 32 cores per node. On the right side we show the scaling over multiple nodes on HOREKA (2x Intel Xeon Platinum 8368, InfiniBand 4X HDR 200 GBit/s interconnect). The I/O of our calculations is negligible compared to the clusters capabilities. The code shows almost no dependence on the amount of nodes used. Both results are for ^{16}O in

a box of size $L^3 = 10^3$ and $L_t = 100$ in lattice units (that is in terms of the spatial and the temporal lattice spaching, in order).

For large applications using up to 64 nodes is favourable compared to 128. Therefore a typical calculation usually uses 64 nodes corresponding to 4864 processes rather than 128 nodes. For the calculation of hypernuclei and multi-strangeness matter which require a large number of jobs also smaller job sizes have been used.

The code is parallelized utilizing MPI for communication within a node as well as internode communication. Hyper-threading does not increase the performance and is therefore not used. GPU codes are parallelized using MPI/CUBLAS and custom kernels in CUDA-FORTRAN.

In total we used about 49 million CPU hours on Horeka during the last funding period. About 50% of this budget are used for calculating multi-strangeness matter and hypernuclei. The rest of time is split roughly evenly between the other projects. In addition we used about 13000 GPU hours to start to develop new interactions in the hypernuclear sector. For the projects presented here an additional 10 million core hours have been used on the JUWELS-Cluster Module (2× Intel Xeon Platinum 8168 CPU, InfiniBand) at the Jülich Supercomputing Centre.

Appendix B: List of publications achieved during this funding period

- Ulf-G. Meißner, Bernard Ch. Metsch, Helen Meyer, *Fine-tunings in radiative α-particle capture on 12C at astrophysical energies*, arxiv: 2601.11180 [nucl-th], DOI: 10.1088/1572-9494/ae69c7, accepted in Communications in Theoretical Physics.

- Shuang Zhang, Serdar Elhatisari, and Ulf-G. Meißner, *Multi-neutron correlations in light nuclei via ab-initio lattice simulations*, arXiv:2512.18849 [nucl-th], DOI: 0.48550/arXiv.2512.18849, submitted for publication.

- Hui Tong, Serdar Elhatisari, Ulf-G. Meißner, and Zhengxue Ren, *Multi-strangeness matter from ab initio calculations*, arXiv:2509.26148, DOI: 10.48550 /arXiv.2509.26148, submitted for publication.

- Serdar Elhatisari, Fabian Hildenbrand, and Ulf-G. Meißner, *Ab initio lattice study of neutron–alpha scattering with chiral forces at N3LO*, J. Phys. G **52** (2025) 12, 125102, DOI: 10.1088/1361-6471/ae2145.

- Zhengxue Ren, Serdar Elhatisari, and Ulf-G. Meißner, *Ab Initio Study of the Radii of Oxygen Isotopes*, Phys. Rev. Lett. **135** (2025) 15, 152502, DOI: 10.1103/y6s2-43ym.

References

1. T. A. Lähde and U.-G. Meißner, "Nuclear Lattice Effective Field Theory: An introduction," Lect. Notes Phys. **957** (2019), 1-396 Springer, 2019.
2. J. W. Chen, D. Lee and T. Schäfer, "Inequalities for light nuclei in the Wigner symmetry limit," Phys. Rev. Lett. **93** (2004), 242302 [arXiv:nucl-th/0408043 [nucl-th]].
3. A. Cipollone, C. Barbieri and P. Navrátil, "Chiral three-nucleon forces and the evolution of correlations along the oxygen isotopic chain," Phys. Rev. C **92** (2015) no.1, 014306 [arXiv:1412.0491 [nucl-th]].
4. V. Lapoux, V. Somà, C. Barbieri, H. Hergert, J. D. Holt and S. R. Stroberg, "Radii and Binding Energies in Oxygen Isotopes: A Challenge for Nuclear Forces," Phys. Rev. Lett. **117** (2016) no.5, 052501 [arXiv:1605.07885 [nucl-ex]].
5. P. Maris *et al.* [LENPIC], "Nuclear properties with semilocal momentum-space regularized chiral interactions beyond N2LO," Phys. Rev. C **106** (2022) no.6, 064002 [arXiv:2206.13303 [nucl-th]].
6. S. Elhatisari, L. Bovermann, Y. Z. Ma, E. Epelbaum, D. Frame, F. Hildenbrand, M. Kim, Y. Kim, H. Krebs and T. A. Lähde, *et al.* "Wavefunction matching for solving quantum many-body problems," Nature **630** (2024) no.8015, 59-63 [arXiv:2210.17488 [nucl-th]].
7. S. Elhatisari, E. Epelbaum, H. Krebs, T. A. Lähde, D. Lee, N. Li, B. n. Lu, U.-G. Meißner and G. Rupak, "Ab initio Calculations of the Isotopic Dependence of Nuclear Clustering," Phys. Rev. Lett. **119** (2017) no.22, 222505 [arXiv:1702.05177 [nucl-th]].
8. Z. Ren, S. Elhatisari and U. G. Meißner, "Ab Initio Study of the Radii of Oxygen Isotopes," Phys. Rev. Lett. **135** (2025) no.15, 152502 [arXiv:2506.02597 [nucl-th]].
9. S. Quaglioni and P. Navratil, "Ab initio many-body calculations of nucleon-nucleus scattering," Phys. Rev. C **79** (2009), 044606 [arXiv:0901.0950 [nucl-th]].
10. S. Elhatisari, F. Hildenbrand and U.-G. Meißner, "Ab initio lattice study of neutron–alpha scattering with chiral forces at N3LO," J. Phys. G **52** (2025) no.12, 125102 [arXiv:2507.08495 [nucl-th]].
11. M. Lüscher, "Two particle states on a torus and their relation to the scattering matrix," Nucl. Phys. B **354** (1991), 531-578.
12. G. M. Hale, "Private communication," (2023).
13. F. M. Marqués and J. Carbonell, "The quest for light multineutron systems," Eur. Phys. J. A **57** (2021) no.3, 105 [arXiv:2102.10879 [nucl-ex]].
14. S. Zhang, S. Elhatisari and U.-G. Meißner, "Multi-neutron correlations in light nuclei via ab-initio lattice simulations," [arXiv:2512.18849 [nucl-th]].
15. H. Tong, S. Elhatisari, U.-G. Meißner and Z. Ren, "Multi-strangeness matter from ab initio calculations," [arXiv:2509.26148 [nucl-th]].
16. P. Eckert and P. Achenbach, "Chart of hypernuclides - hypernuclear structure and decay data," (2023) `https://hypernuclei.kph.uni-mainz.de/`
17. A. Di Donna, L. Contessi, A. Lovato and F. Pederiva, "Hypernuclei with neural network quantum states," Phys. Rev. Res. **8** (2026) no.1, 013160 [arXiv:2507.16994 [nucl-th]].
18. M. Knöll and R. Roth, "Hyperon-nucleon interaction constrained by light hypernuclei," Phys. Lett. B **846** (2023), 138258 [arXiv:2307.11577 [nucl-th]].
19. D. Sloan, R. Alves Batista, M. T. Hicks and R. Davies, "Fine-Tuning in the Physical Universe," Cambridge University Press, 2020.
20. U.-G. Meißner, B. C. Metsch and H. Meyer, "The electromagnetic fine-structure constant in primordial nucleosynthesis revisited," Eur. Phys. J. A **59** (2023) no.10, 223 [arXiv:2305.15849 [hep-th]].
21. T. A. Lähde, U.-G. Meißner and E. Epelbaum, "An update on fine-tunings in the triple-alpha process," Eur. Phys. J. A **56** (2020) no.3, 89 [arXiv:1906.00607 [nucl-th]].
22. S. I. Ando, "Cluster effective field theory and nuclear reactions," Eur. Phys. J. A **57** (2021) no.1, 17 [arXiv:2011.07207 [nucl-th]].
23. U.-G. Meißner, B. C. Metsch and H. Meyer, "Fine-tunings in radiative α-particle capture on ^{12}C at astrophysical energies," [arXiv:2601.11180 [nucl-th]].